

Article

# Enhancement of Mechanical Properties of Hot-Forged 6082 Suspension Parts via Rapid IR Heat Treatment

Yi-Ling Chang , Fei-Yi Hung \*  and Truan-Sheng Lui

Department of Materials Science and Engineering, National Cheng Kung University, Tainan 701, Taiwan; lingiscute@gmail.com (Y.-L.C.); luits@mail.ncku.edu.tw (T.-S.L.)

\* Correspondence: fyhung@mail.ncku.edu.tw; Tel.: +886-6-2757-5756-2950

Received: 25 May 2018; Accepted: 28 June 2018; Published: 29 June 2018



**Abstract:** Post-forging heat treatment is often necessary to achieve the mechanical properties required for aluminum alloy forged parts. In this study, hot-forged 6082 suspension parts are used to study the effect of rapid infrared (IR) heat treatment. The insoluble particles present in the matrix after the solutionizing process are observed. Experimental results show that using rapid IR heat treatment leads to superior solutionizing, and thus a larger critical onset strain in serrated tensile flow. The rapid IR heat treatment also had a more significant precipitation effect, which enhanced the mechanical properties of the material.

**Keywords:** rapid infrared (IR) heat treatment; 6082 suspension parts; forging; solutionization; critical onset strain

## 1. Introduction

Among 6xxx (Al–Mg–Si) series aluminum alloys, 6082 aluminum alloy has a very attractive combination of light weight, high strength, corrosion resistance, and high recyclability [1]; hence, they had been widely used in the automotive industry, for instance, in automobile suspension components. The main additives for 6082 aluminum alloy are magnesium (Mg) and silicon (Si), with Fe, Mn, and Cr used as additional elements to enhance properties (e.g., tensile strength and grain size control) [2].

Most automobile suspension components are manufactured using a high-temperature forging process, which allows the production of high-precision near-net shape parts. The forging process changes the microstructure and mechanical properties of the material [3]. Although grains are prone to grow in the subsequent heat treatment [4], 6082 aluminum alloys are heat-treated to increase their strength, impact resistance, and toughness [5]. Thus, the subsequent heat treatment, called post-forging heat treatment (PFHT), is indispensable.

In the PFHT process, a solution heat treatment and the artificial aging is included. In the solution heat treatment process, once the material is held at an elevated temperature for a sufficient time, all the constituents (e.g., Al–Mg–Si phases) are taken into solid solution, producing a single phase. A supersaturated solid solution (S.S.S.S) forms after water quenching. Aging heat treatment then leads to the formation of finely dispersed precipitates, modifying the required mechanical properties. The precipitation sequence for 6xxx alloys is generally: S.S.S.S → Mg clusters, Si clusters and Mg–Si co-clusters → Guinier–Preston (GP) zones →  $\beta''$  →  $\beta'$  and B phase →  $\beta$  ( $Mg_2Si$ , stable), where the most effective hardening phase is  $\beta''$  [6,7]. However, a typical PFHT cycle may take many hours, thus, a rapid heat treatment method is thus urgently needed. To curtail the PFHT duration, many heat treatment methods had been investigated.

Fluidized bed solution treatment is used as a rapid heat treatment method for Al–Mg–Si alloys [8]. However, the heat transfer media used in the fluidized bed (fine hard media, such as sand) is

inconvenient for reheating and recycling. Using a salt bath method can reduce the duration of heat treatment and enhance the yield strength of 6082 extruded specimens [9]. However, salt bath heating is a liquid state heating method, and there is a danger that the salt particles will erupt and explode due to rapid cooling by water, causing a potential safety problem, and thus has been banned in many countries. Additionally, rapid infrared (IR) heating method had been used as a rapid heating method to curtail the pre-heating duration of forging process [9], in an IR heating furnace, heat transfer occurs via convection and radiation. The method is thus clean and has a rapid heating rate and accurate temperature control [10]. According to our previous study, it had been found that using rapid IR heating method could curtail the duration of PFHT of 6082 forgings [11]. However, in that study, the effect of IR heat treatment on hot-forged 6082 aluminum alloy has not been clarified, especially that of IR rapid heating on 6082 real body forgings. This investigation also determines the critical parameters for PFHT of 6082 real body forgings.

## 2. Experiments

Hot-forged 6082 suspension parts were used as the study material. Figure 1a shows a photograph of the real body 6082 forged parts. The chemical composition of the forgings is given in Table 1. The sampling location is shown in Figure 1b.

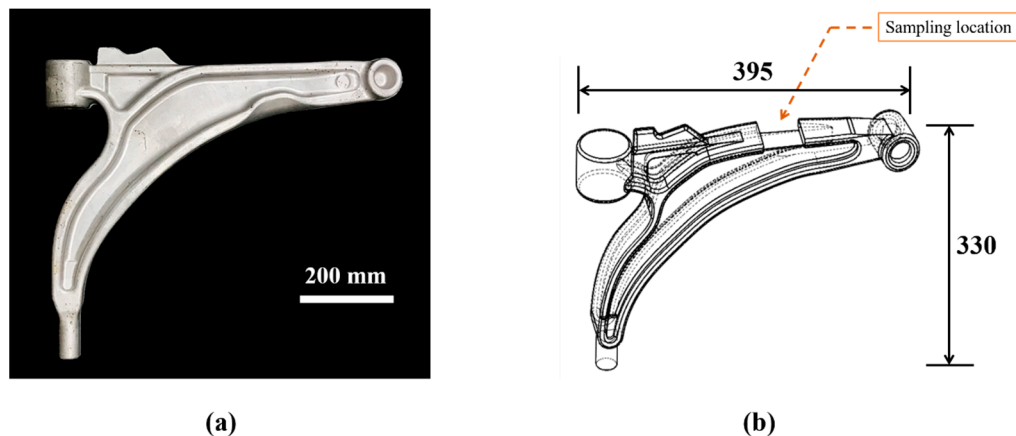


**Figure 1.** (a) Photograph of real body 6082 aluminum forging and (b) the diagram of sampling location (all dimensions are in mm).

**Table 1.** Chemical composition of 6082 aluminum alloy.

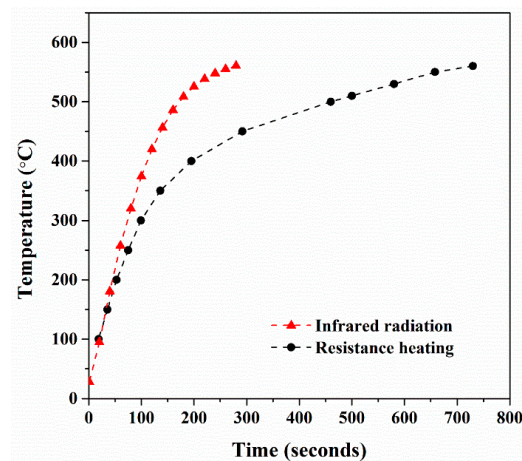
Element	Mg	Si	Cu	Mn	Cr	Fe	Zr	Al
wt. %	1.07	1.18	0.09	0.90	0.14	0.24	0.001	Bal.

Forged parts were heated using conventional heat treatment (resistance heating, RH) and IR heat treatment, respectively. Typical solution temperatures and times were utilized to establish baseline information. To replace the conventional heat treatment, the longest duration for solution heat treatment was controlled to be less than 2 h. The experimental parameters and codes are shown in Table 2.

In addition, the comparison of temperature profiles between specimen heated in RH furnace and that heated in IR furnace is showed in Figure 2.

**Table 2.** Experimental parameters and specimen codes.

Code	Solution Heat Treatment	Artificial Aging
RH10	RH, 560 °C, 10 min	-
RH30	RH, 560 °C, 30 min	-
RH120	RH, 560 °C, 120 min	-
IR10	IR heating, 560 °C, 10 min	-
IR30	IR heating, 560 °C, 30 min	-
IR120	IR heating, 560 °C, 30 min	-
RH30-2H	RH, 560 °C, 30 min	RH, 180 °C, 2 h
RH30-6H	RH, 560 °C, 30 min	RH, 180 °C, 6 h
IR30-6H	IR, 560 °C, 30 min	IR, 180 °C, 6 h

**Figure 2.** Comparison of temperature profiles between specimen heated in resistant heat (RH) furnace and that heated in IR furnace.

The measurement conditions for Rockwell hardness followed the B-scale. The mean value for five impressions was taken as the hardness of the corresponding condition. The microstructure and secondary phase of the alloy after heat treatment were observed using optical microscopy (OM; OLYMPUS BX41M-LED, OLYMPUS, Tokyo, Japan) and scanning electron microscopy (SEM; HITACHI SU-5000, HITACHI, Tokyo, Japan) with energy-dispersive X-ray spectrometry (EDS; EDAX, Singapore, Singapore). For the OM observations, the samples were ground using SiC papers, from #120 to #4000, and polished in an Al<sub>2</sub>O<sub>3</sub> aqueous suspension (1.0 and 0.3 μm) and an SiO<sub>2</sub> polishing suspension and then etched using Keller's reagent and KMnO<sub>4</sub>. To quantify the microstructural changes after solution treatment, an image analysis method was applied to determine the area fraction of the secondary phase, which were measured using ImageJ software (National Institutes of Health, Bethesda, MD, USA, version: 1.48), where each value was calculated from 10 images. X-ray diffraction (XRD; Bruker AXS GmbH, Karlsruhe, Germany) analysis with Cu Kα radiation was employed in the 2θ range of 10° to 60° to identify the secondary compounds. Microstructural feature (precipitates) observations were carried out using transmission electron microscopy (TEM; Tecnai F20 G2, EFI, Hillsboro, OR, USA). The specimen of tensile test is cut from the sampling location (showed in Figure 1b) by wire electrical discharge machining method. The dimensions of the tensile test specimen are shown in Figure 3. Tensile tests were performed using a universal testing machine in air at room temperature. And the strain rate is  $1.66 \times 10^{-3} \text{ s}^{-1}$ .

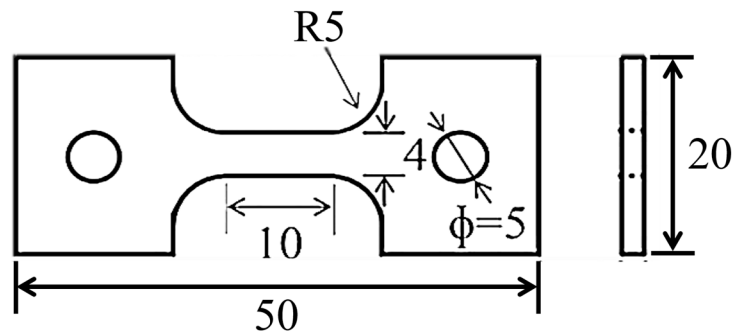


Figure 3. Schematic diagram of tensile test specimens (all dimensions are in mm).

The tensile testing of the as-quenched specimens was conducted after 10 min (T4 condition). TEM, XRD, and SEM analyses on the samples were conducted after 7 days of natural aging.

### 3. Results and Discussion

#### 3.1. Effect of IR Heating on Solutionization

Figure 4a shows the hardness profiles of the solutionized specimens after water quenching. Initially, the IR-heated specimens have higher hardness than that of RH-heated specimens. Figure 4b shows the hardness of the specimens after 7 days of natural aging. The common solution heat treatment time for 6082 aluminum alloy is 120 min [9,11]. On both IR-heated specimens and RH-heated specimens, the hardness values become identical after 30 min of solutionizing. And after 7 days natural aging, specimen IR30 has the highest hardness value, showing that the higher heating up rate leads to a better hardenability. The results also show that the best solutionization time for IR heating, among the conditions tested, is 30 min. However, it is inadequate to measure the effectiveness of solution heat treatment only by hardness. As a result, calculation of the second phases area fraction and the mechanical properties after T4 and T6 heat treatment were performed in the followed experiment.

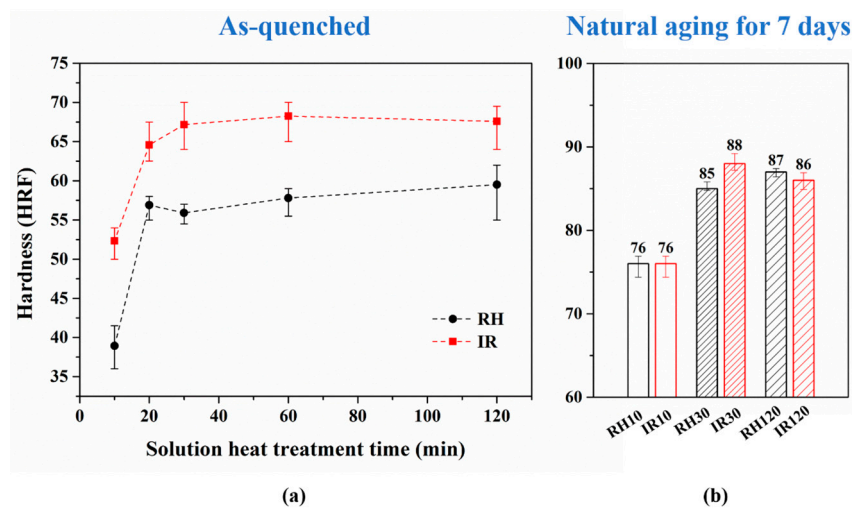
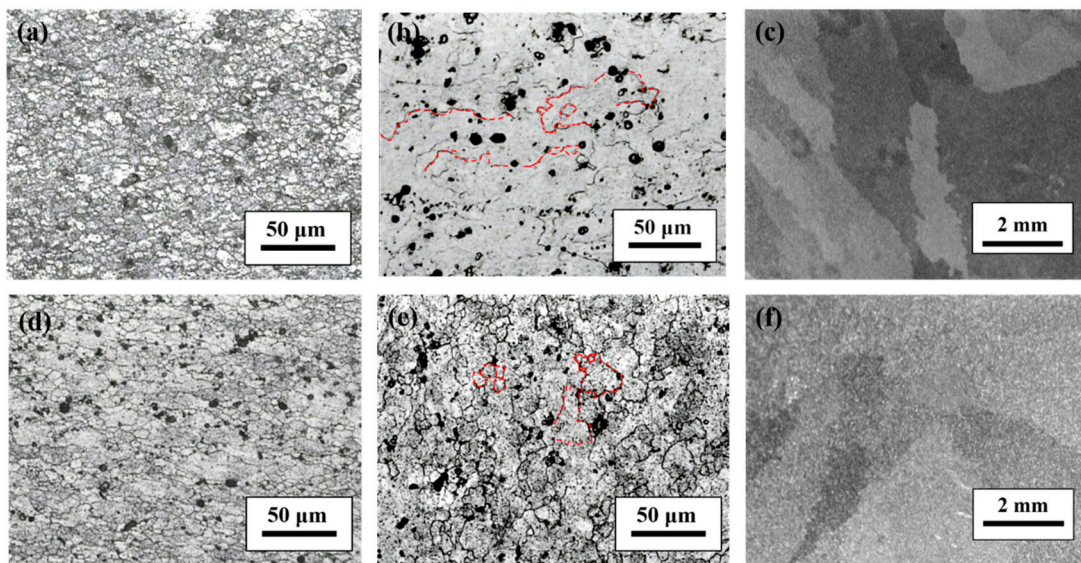


Figure 4. Hardness of various heat-treated specimens of (a) as-quenched; (b) natural aging for 7 days.

Figure 5 shows metallographic images of various heat-treated specimens.



**Figure 5.** Microstructural features of (a) RH10; (b) RH30; (c) RH120; (d) IR10; (e) IR30; and (f) IR120.

On the IR10 and RH10 specimens, lots of recrystallized grains can be observed; these grains formed during the hot working process (dynamic recrystallization during extrusion and forging). With the solution heat treatment duration prolonged to 30 min, some of these dynamically recrystallized grains became coarse, with the grains in RH30 coarser than those in IR30. Further coarsening was observed when the duration was prolonged to 120 min (IR120 and RH120).

Figure 6 shows the microstructural features of RH-heated and IR-heated specimens. The dark and gray secondary phases tend to decrease after solution heat treatment (Figure 7).

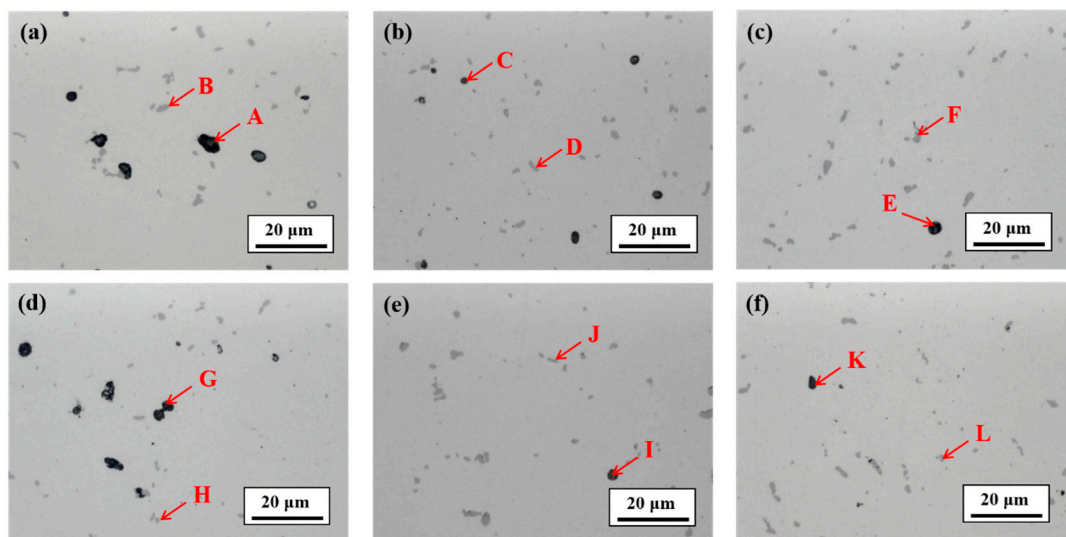


**Figure 6.** Secondary phase observations of (a) RH10; (b) RH30; (c) RH120; (d) IR10; (e) IR30; and (f) IR120.

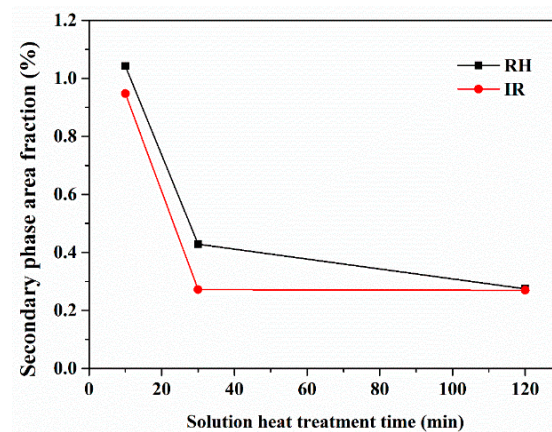


**Figure 7.** Area fractions of Al–Mg–Si phase and Al(FeMnCr)Si secondary phases.

The results of EDS analysis, which focused on secondary phases, are shown in Tables 3 and 4. The gray secondary phases were Al(FeMnCr)Si phases, and the dark phases were Al–Mg–Si phases. Based on the results of Figure 7, the decrease in the secondary phase area fraction is due to the solutionization of Al–Mg–Si phases. It should also be noted that the secondary phase area fraction of IR10 was lower than that of RH10, and that of IR30 was lower than that of RH30; IR30 had the same secondary phase area fraction as those of RH120 and IR120. Thus, it is reasonable to suggest that IR heating produces a better solutionizing effect of Al–Mg–Si phases than does RH. From the results of hardness (Figure 4) and the secondary phase area fraction results (Figure 7), 30 min of IR heat treatment is sufficient to reach the maximum solution effect (at 560 °C) of the alloy.

**Table 3.** Energy-dispersive X-ray spectrometry analysis results for RH-heated specimens.

Sample Condition	RH10		RH30		RH120	
	A	B	C	D	E	F
Fe	0.07	2.54	0.08	3.58	0.54	2.96
Cu	0.21	0.33	0.15	0.34	0.95	0.77
Mg	45.13	1.41	3.65	1.55	9.75	1.87
Al	28.75	72.74	37.76	71.04	65.06	82.45
Si	22.01	9.36	54.01	9.91	22.71	7.20
Cr	2.24	2.92	2.91	3.42	0.56	0.80
Mn	1.59	10.69	1.45	10.15	0.43	3.95

**Table 4.** EDS analysis results for IR-heated specimens.

Sample Condition	IR10		IR30		IR120	
	G	H	I	J	K	L
Fe	0.42	0.48	0.81	4.02	0.28	5.16
Cu	1.00	1.00	1.69	1.59	0.42	0.82
Mg	33.71	1.71	2.68	1.62	1.83	0.93
Al	36.49	81.17	91.96	79.24	94.90	73.49
Si	27.16	6.77	1.15	7.23	1.93	9.17
Cr	0.65	0.45	0.61	1.36	0.39	0.79
Mn	0.58	0.77	1.09	4.95	0.25	0.74

The XRD results for the IR- and RH-heated specimens are shown in Figure 8. The results show that with prolonged solution heat treatment duration, the signal of the Al–Mg–Si primary phase (at 40.2°) decreased and that of Al(FeMnCr)Si became obvious. However, it is hard to distinguish the difference between RH and IR specimens.

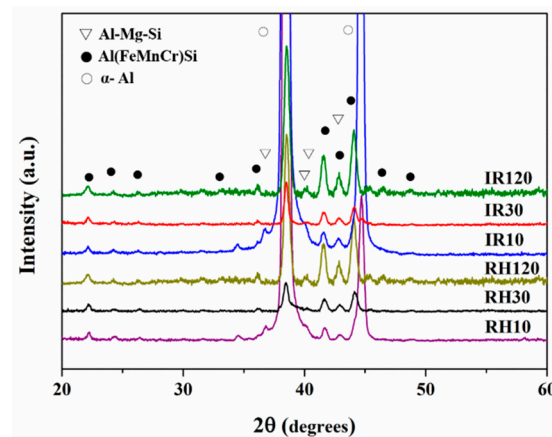


Figure 8. X-ray diffraction patterns of specimens treated under various solution heat treatment conditions.

Figure 9 shows the tensile deformation flow curves for RH30 and IR30. The tensile strength (ultimate tensile strength (UTS) and yield strength (YS)) of IR30 is higher than that of RH30. Significant serrated flow due to dynamic strain aging (DSA) was found for both RH30 and IR30. The mechanism of DSA is related to the concentration of the solute solution and the precipitates [12,13]. A comparison of the critical onset strain ( $\epsilon_c$ ) of serrated flow shows that  $\epsilon_c$  tends to increase for specimens subjected to IR heating.

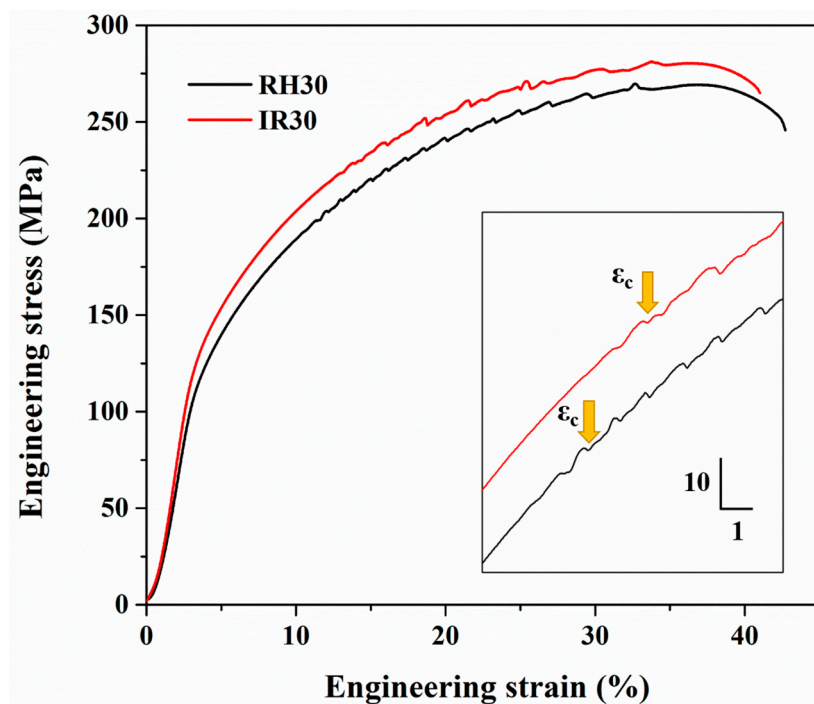


Figure 9. Effect of heating rate before solutionization on critical onset strain ( $\epsilon_c$ ) of tensile serrated flow curve of 6082 forging specimens.

According to studies on Al-Mg alloy [14], with increasing concentration of solid solution Mg atoms in the matrix, and with the follow-up precipitation process, the critical onset strain ( $\epsilon_c$ ) increases. Thus, a comparison of the onset strain ( $\epsilon_c$ ) to the tensile strength and hardness values (Figure 4) and the secondary phase observation results (Figure 7) reveals that the IR30 specimen had the highest concentration of Mg and Si atoms in the matrix, and thus the largest amount of dynamically formed precipitates in the tensile test. These Mg and Si atoms and dynamically formed precipitates have strong

solute interactions and impede the formation of a dislocation atmosphere, increasing the hardness and the strength. Figure 10 shows TEM images of IR30 and RH30. There are some unsolutionized secondary phases in the matrix of RH30, implying that IR heating leads to more complete solutionization, and this observation result implying the same result as mentioned above.

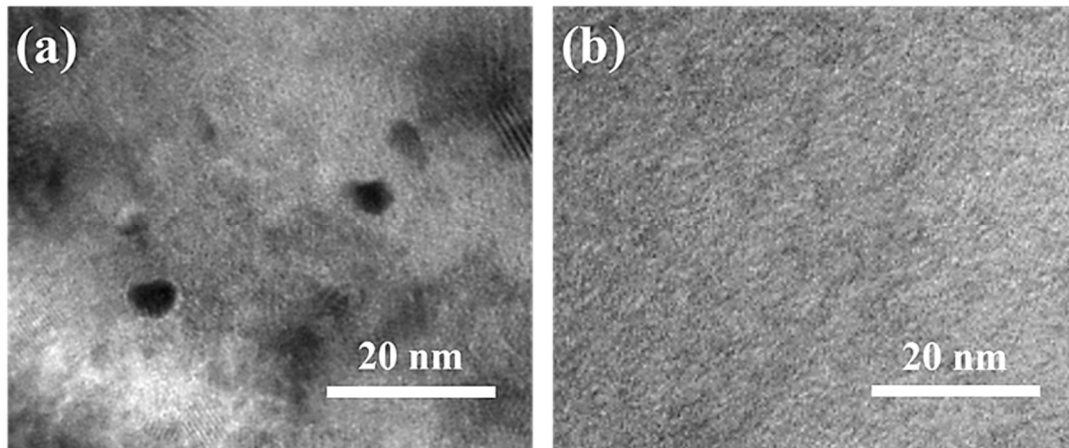


Figure 10. Transmission electron microscopy images of (a) RH30 and (b) IR30.

### 3.2. Effect of Rapid IR Solutionization on T6 Process

Figure 11 shows the hardness profiles of aged specimens. The IR-heated specimens initially show better hardening rates than those of RH-heated specimens, and achieve a peak aging condition within 2 h. However, the peak hardness values were eventually almost identical for all solutionization heating rates.

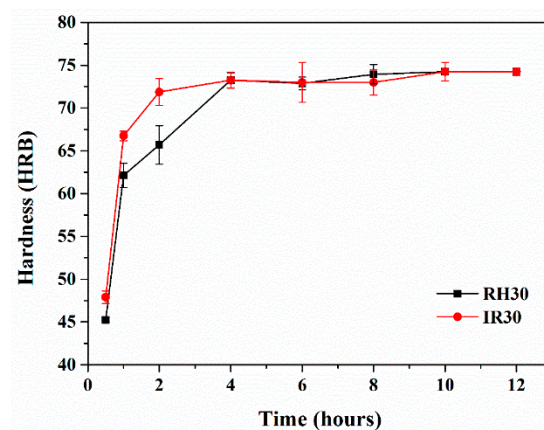
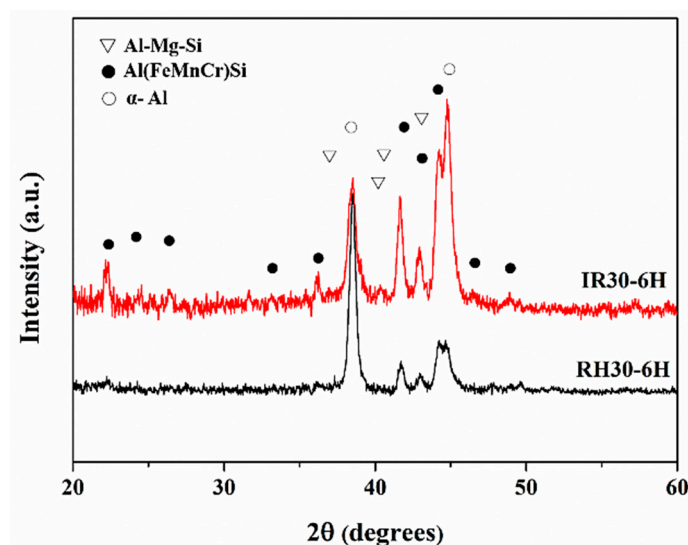


Figure 11. Effect of IR heat treatment on hardness profiles of specimens aged at 180 °C.

Figure 12 shows the results of XRD analysis. The peaks of Al–Mg–Si and Al(FeMnCr)Si can be detected, and the IR30-6H specimen showed more obvious secondary phases/precipitates signal than the RH30-6H condition.



**Figure 12.** XRD patterns of A6082 alloys treated under various T6 heat treatment conditions.

In order to determine the best heat treatment parameter settings, the tensile test results of RH30-6H, IR30-2H, and IR30-6H are shown in Table 5. Compared to RH30-6H, IR30-2H has a similar ultimate tensile strength (UTS) but a lower yield strength (YS). The yield and ultimate tensile strength of IR30-6H are higher than those of RH30-6H. According to our previous experiment, using a rapid solution heat treatment method (salt bath) can increase strength [9]. Thus, it is reasonable to suggest that the IR-heated specimen achieved higher tensile strength due to rapid solutionization. To sum up, using IR heating as a rapid heating method leads to better solutionization, reduces the required duration of the PFHT process, maintains a small grain, and increases tensile strength.

However, the requirement for a commercial suspension part is not only a high tensile strength (YS > 285 MPa, UTS > 340 MPa) but also an adequate tensile elongation of 8–10%. Hence, even the peak aging condition of IR heat treatment can provide a superior tensile strength, the elongation is slightly inadequate. Comparing the IR-heated samples, IR30-2H had a lower tensile yield strength compared to that of IR30-6H but better tensile elongation. Hence, four hours of aging might be optimal for industrial applications.

**Table 5.** YS, UTS, UE, and TE values and strain hardening exponent obtained from tensile test curves.

Sample	Yield Strength (YS)	Ultimate Tensile Strength (UTS)	Uniform Elongation (UE)	Total Elongation (TE)	Strain Hardening Exponent, $n$	Coefficient of Determination, $R^2$
RH30	115	270	26	37	0.32	0.9995
IR30	125	281	27	34	0.29	0.9987
RH30-6H	328	360	6	10	0.09	0.9994
IR30-2H	305	364	12	13	0.08	0.9995
IR30-6H	366	390	7	8	0.11	0.9965

Figure 13a–d shows TEM images and selected area diffraction patterns (SADP) of IR30-6H and RH30-6H specimens. The IR30-6H specimen has a larger amount of precipitates, and the precipitates in RH30-6H ( $15.9 \pm 3.5$  nm) are longer than those in IR30-6H ( $12.4 \pm 3.0$  nm). According to previous research and the selected area diffraction patterns, the precipitates in RH30-6H and IR30-6H specimens belong to the stage in which the GP zone ( $\sim 1\text{--}3$  nm; coherent to the matrix) transforms into the  $\beta''$  phase ( $\sim 4 \times 4 \times 50$  nm<sup>3</sup>), which is semi-coherent to the matrix [15]. Considering the coherence effect of the precipitates and the matrix [16,17], the precipitates in RH30-6H are less coherent than those in IR30-6H; however, IR30-6H has a larger amount of precipitates. Hence, a possible explanation for the better precipitate hardening effect observed in IR30-6H compared to that in RH30-6H is the large amount of precipitates, and caused a better tensile strength (as showed in Table 5).

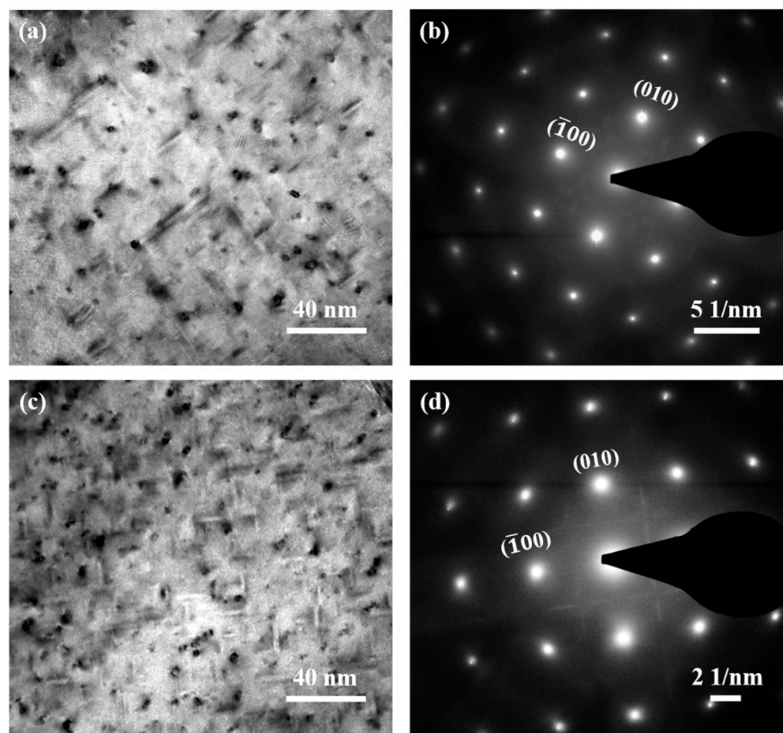


**Figure 13.** TEM images (a) bright field image of RH30-6H; (b) selected area diffraction pattern (SAPD) image of RH30-6H; (c) bright field image of IR30-6H; (d) SAPD image of IR30-6H.

### 3.3. Effect of Rapid IR Solutionization on Tensile Deformation and Fracture Features

Figure 14 shows the fracture surfaces after the tensile test. The fracture surface of specimens is composed of many dimples, which suggests that the fracture mechanism is ductile fracture. There is no significant difference between the RH-heated and IR-heated samples.

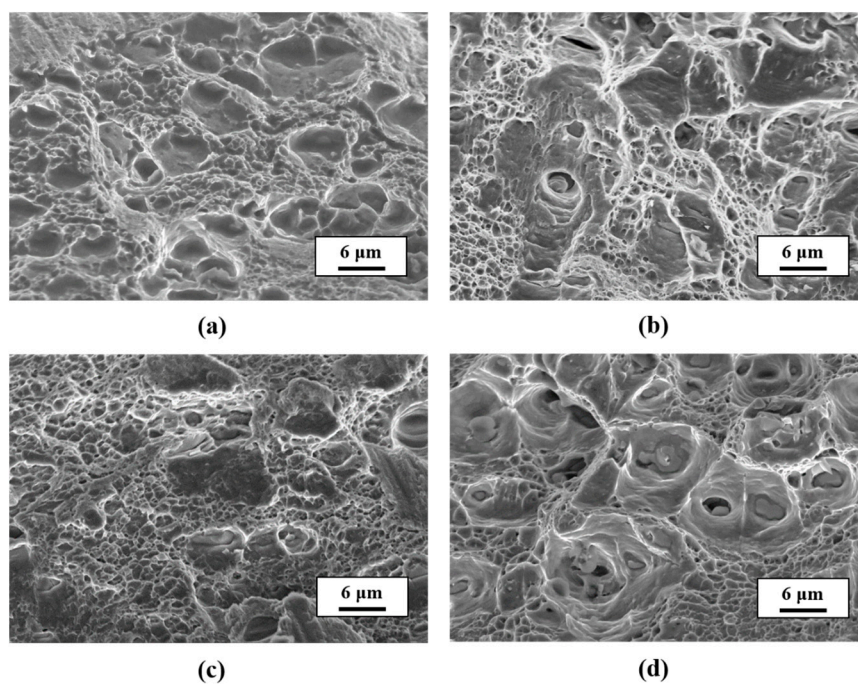


**Figure 14.** Fracture images of (a) RH30; (b) IR30; (c) RH30-6H; and (d) IR30-6H.

To evaluate the work hardening ability and behavior of IR-heated samples, the  $n$  value (strain hardening exponent) were estimated (Table 5). The  $n$  value is used to evaluate the work hardening ability and necking resistance [18]. The  $n$  values for RH30 and IR30 are similar (0.32 vs. 0.29, respectively). The strain hardening exponents for RH30-6H and IR30-6H are 0.09 and 0.11, respectively. The strain-hardening exponent of T6 samples is lower than those of RH30 and IR30. This is due to the formation of precipitates, which cause uneven deformation but still increased strength.

The results show that using IR heating as a rapid heating method leads to better solutionization, reduces the required duration of the PFHT process, maintain small grains, and increases tensile strength. However, the requirement for a commercial suspension part is not only a high tensile strength (YS > 285 MPa, UTS > 340 MPa) but also a sufficient tensile elongation of 8–10% [19]. Hence, even the peak aging condition of IR heat treatment can provide a superior tensile strength, the elongation is slightly inadequate. Comparing the IR-heated samples, IR30-2H had a lower tensile yield strength compared to that of IR30-6H but better tensile elongation. Hence, four hours of aging might be optimal for industrial applications.

Using IR heating as a rapid heating method leads to higher hardness. And with the increasing of solution heat treatment duration, the fraction of Al–Mg–Si phases decreased. It should be also noted that the solutionizing rate of Al–Mg–Si phases by IR-heated faster than the RH-heated specimens. On the other hand, the critical grain size of RH-heated specimen could be observed in the earlier stage of solutionizing.

Besides, using IR heating as a PFHT method can attain a higher solutionizing level, acquire more precipitates and achieve a higher tensile strength. The microstructural features and hardness evolution of 6082 forged samples after different solutionizing methods are plotted in Figure 15. The possible mechanism of rapid IR heating is plotted in Figure 16.

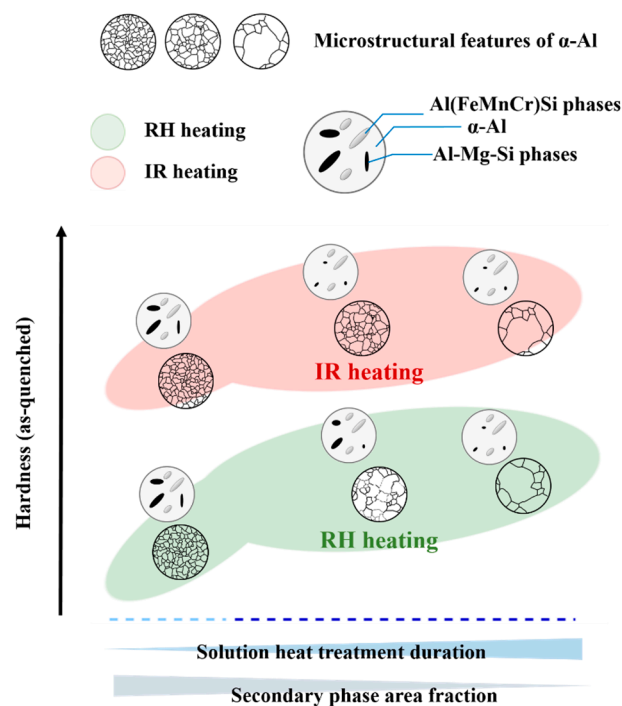


**Figure 15.** Evolution of microstructure and hardness during rapid heating process.

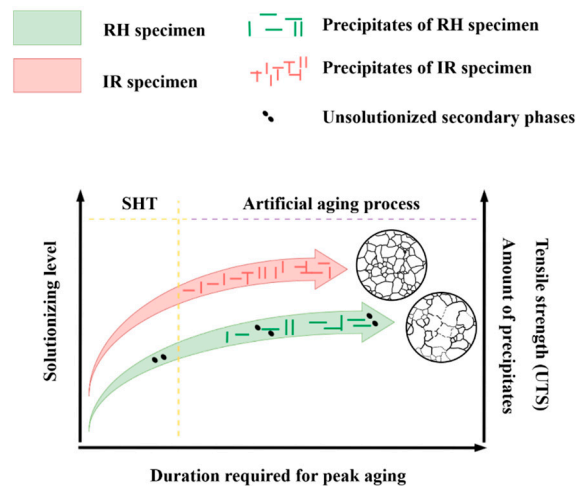


**Figure 16.** Schematic diagram of rapid heating process. Process can be applied to acquire larger amount of precipitates and slightly higher tensile strength.

#### 4. Conclusions

In this study, IR heat treatment was used as a rapid heat treatment method for 6082 suspension parts. Using IR rapid heating can reduce the duration of the solutionizing process to 30 min. Experimental results confirmed that the critical onset strain ( $\epsilon_c$ ) of tensile serrated flow is a useful parameter related to amount of Mg and Si atoms in solid solution.

For aged specimens, the hardness profiles and tensile test data indicate that IR rapid heating can increase the effect of aging. The peak aging condition was achieved in 2 h. IR-heated specimens showed a more predominant precipitation effect than did RH-heated specimens, and showed higher tensile strength; however, their fracture features were still mainly those of ductile fracture and the work hardening behavior remained unchanged.

The results obtained in this study show that IR heating can be considered as a potential method for rapid solutionization. The results can be used as a reference for industrial applications.

**Author Contributions:** Y.-L.C. performed the experiments, analyzed the data, and wrote the paper. F.-Y.H. and T.-S.L. are advisers.

**Funding:** This research received no external funding.

**Acknowledgments:** The authors are grateful to the Instrument Center of National Cheng Kung University and the Ministry of Science and Technology of Taiwan (Grant No. MOST 106-2221-E-006-064) for their financial support.

**Conflicts of Interest:** The authors declare no conflict of interest.

#### References

1. Das, S.K. Designing aluminium alloys for a recycling friendly world. *Mater. Sci. Forum* **2006**, *519–521*, 1239–1244. [[CrossRef](#)]
2. Lillywhite, S.; Prangnell, P. Interactions between precipitation and recrystallisation in an Al–Mg–Si alloy. *Mater. Sci. Technol.* **2000**, *16*, 1112–1120. [[CrossRef](#)]
3. Birol, Y. Effect of extrusion press exit temperature and chromium on grain structure of EN AW 6082 alloy forgings. *Mater. Sci. Technol.* **2015**, *31*, 207–211. [[CrossRef](#)]
4. Birol, Y.; Ilgaz, O. Effect of cast and extruded stock on grain structure of EN AW 6082 alloy forgings. *Mater. Sci. Technol.* **2014**, *30*, 860–866. [[CrossRef](#)]
5. Mrówka-Nowotnik, G.; Sieniawski, J. Effect of heat treatment on tensile and fracture toughness properties of 6082 alloy. *J. Achiev. Mater. Manuf. Eng.* **2009**, *32*, 162–170.
6. Mrówka-Nowotnik, G.; Sieniawski, J. Influence of heat treatment on the microstructure and mechanical properties of 6005 and 6082 aluminium alloys. *J. Mater. Process. Technol.* **2005**, *162*, 367–372. [[CrossRef](#)]

7. Zhen, L.; Fei, W.D.; Kang, S.B.; Kim, H.W. Precipitation behaviour of Al–Mg–Si alloys with high silicon content. *J. Mater. Sci.* **1997**, *32*, 1895–1902. [[CrossRef](#)]
8. Keist, J. The development of a fluidized bed process for the heat treatment of aluminum alloys. *JOM* **2005**, *57*, 34–39. [[CrossRef](#)]
9. Chang, Y.L.; Hung, F.Y. Enhancing the tensile yield strength of A6082 aluminum alloy with rapid heat solutionizing. *Mater. Sci. Eng. A* **2017**, *702*, 438–445. [[CrossRef](#)]
10. Kadolkar, P.B.; Lu, H. Application of rapid infrared heating to aluminum forgings. In Proceedings of the 25th Forging Industry Technical Conference of the Forging Industry Association and the Forging Industry Educational and Research Foundation 2004, Detroit, MI, USA, 19–21 April 2004.
11. Chang, Y.L.; Hung, F.Y. Study of microstructure and tensile properties of infrared-heat-treated cast-forged 6082 aluminum alloy. *J. Mater. Res. Technol.* **2017**, in press. [[CrossRef](#)]
12. Chan, K.; Lui, T. Portevin-lechatelier effect of Al-7 mass% Si-Mg cast alloys. *Mater. Trans.* **1995**, *36*, 615–619. [[CrossRef](#)]
13. Chan, K.S.; Lui, T.S. Temperature Dependence of the Tensile Behavior of Cast and Extruded Al-7Si-0.3 Mg Alloys in 213–673 K. *Mater. Trans.* **1995**, *36*, 743–748. [[CrossRef](#)]
14. Wen, W.; Morris, J. The effect of cold rolling and annealing on the serrated yielding phenomenon of AA5182 aluminum alloy. *Mater. Sci. Eng. A* **2004**, *373*, 204–216. [[CrossRef](#)]
15. Andersen, S.; Zandbergen, H. The crystal structure of the  $\beta''$  phase in Al–Mg–Si alloys. *Acta Mater.* **1998**, *46*, 3283–3298. [[CrossRef](#)]
16. Marioara, C.D.; Andersen, S.J. Atomic model for GP-zones in a 6082 Al–Mg–Si system. *Acta Mater.* **2001**, *49*, 321–328. [[CrossRef](#)]
17. Chen, J.H.; Costan, E. Atomic pillar-based nanoprecipitates strengthen AlMgSi alloys. *Science* **2006**, *312*, 416–419. [[CrossRef](#)] [[PubMed](#)]
18. Zhang, D.; Zhang, D. Excellent ductility and strong work hardening effect of as-cast Mg–Zn–Zr–Yb alloy at room temperature. *J. Alloy Compd.* **2017**, *728*, 404–412. [[CrossRef](#)]
19. Santos, J.; Gouveia, R.M. Designing a new sustainable approach to the change for lightweight materials in structural components used in truck industry. *J. Clean. Prod.* **2017**, *164*, 115–123. [[CrossRef](#)]



© 2018 by the authors. Licensee MDPI, Basel, Switzerland. This article is an open access article distributed under the terms and conditions of the Creative Commons Attribution (CC BY) license (<http://creativecommons.org/licenses/by/4.0/>).